10th International Conference on Composite Science and Technology
ICCST/10
A.L. Araújo, J.R. Correia, C.M. Mota Soares, et al. (Editors)

PROGRESSIVE FAILURE OF PULTRUDED FRP COLUMNS

Francisco Nunes[*], Nuno Silvestre[†] and João R. Correia[*]

[*]CEris, Instituto Superior Técnico, Universidade de Lisboa
Av. Rovisco Pais 1, 1049-001 Lisbon
francisco.nunes@ist.utl.pt; joao.ramoa.correia@ist.utl.pt

[†]LAETA, Instituto Superior Técnico, Universidade de Lisboa
Av. Rovisco Pais 1, 1049-001 Lisbon
nsilvestre@ist.utl.pt

Keywords: Pultruded FRP profiles; progressive failure; numerical modelling; Hashin criterion.

Summary: *This paper presents experimental and numerical investigations about the structural behavior of pultruded fiber reinforced polymer (FRP) columns. Five series of pultruded hybrid profiles with different fiber architectures comprising glass and carbon fibers were designed and tested under compression with three different lengths aiming at studying the local, global and mixed-mode buckling phenomena. The main advantages and drawbacks of introducing carbon fibers in bare glass-FRP (GFRP) profiles were also analyzed. Data obtained in the experimental campaign provided the basis for an extensive numerical study that focused on the progressive failure of the pultruded FRP columns. Linear buckling analyses and progressive failure analyses taking into account the Hashin material damage criterion were carried out using the software ABAQUS. The former analyses allowed determining the linear elastic critical buckling loads and the deformed shapes of each buckling mode, while the latter analyses enabled the simulation of the delamination and (progressive) collapse of the FRP columns. A general good agreement was obtained between the experimental data and numerical results.*

1 INTRODUCTION

Pultruded fiber reinforced polymer (FRP) profiles are finding increasing applications in civil engineering structures due to their advantages over traditional construction materials, such as high strength, lightness and improved durability [1]. The structural behavior of pultruded FRP beams and columns has been extensively investigated in the past by both experimental and numerical means. However, very little information is available regarding the progressive failure mechanisms of those members.

In numerical simulations, the criteria most used to model the ultimate behavior of FRP composite members are only able to predict the failure initiation (*e.g.*, Tsai-Hill, Tsai-Wu, maximum stress and maximum strain). If for some failure mechanisms such criteria usually provide reasonable estimates of the collapse load of FRP members [2], for other types of mechanisms they have been found to largely underestimate the load carrying capacity [3].

This paper presents a numerical study supported by an extensive experimental campaign about the progressive failure of I-section (200×100×10 mm) pultruded FRP columns with different fiber architectures, comprising glass and carbon fibers, tested in compression with three different lengths (600, 1000 and 2000 mm). Three-dimensional finite element models of the columns were

developed using the commercial software ABAQUS by Simulia [4]. Failure progression was modeled using the Hashin material damage criterion that considers the progressive stiffness degradation of the FRP material once the failure initiation criterion is attained. Extensive mechanical characterization tests provided the elastic, strength and fracture properties of the FRP materials. Full-scale column tests allowed validating the numerical models based on the agreement with test. The numerical models were then used to complement the experimental study, namely in terms of stress and strain fields, failure initiation zones and damaged zones.

The remainder of the paper is organized as follows. Section 2 presents the experimental program and summarizes the main results obtained. The numerical models are described in section 3. Next, sections 4 and 5 present the results of the linear buckling analyses and the progressive failure analyses, respectively. The main conclusions drawn from this study are presented in section 6.

2 EXPERIMENTAL PROGRAM AND SUMMARY OF RESULTS

2.1 Experimental series and test setup

Five series of pultruded FRP hybrid profiles (isophthalic polyester matrix) were designed according to the author's previous research [5] and bibliographic review [6]. Four different hybrid prototypes were designed aiming at studying different configurations and architecture of carbon fibers. Two different types of CFRP reinforcement were used in this experimental program: (*i*) unidirectional (0°) 350 g/m^2 CFRP mats, and (*ii*) bidirectional (0°/90°) 400 g/m^2 CFRP mats. Despite the efforts made in using both mats with the same fiber volume, this was the closest match made available by the manufacturer. Thus, the unidirectional and bidirectional mats present a difference of roughly 12.5% in terms of carbon fibers volume.

The introduction of unidirectional or bidirectional CFRP mats in GFRP pultruded profiles has different effects. The former type of CFRP reinforcement, comprising a set of fibers aligned in the 0° direction, provides axial and flexural members with an increase of longitudinal stiffness. On the other hand, bidirectional CFRP mats present fiber filaments oriented in the 0° and 90° directions roughly in the same proportion, thus increasing the longitudinal, transverse and shear stiffness.

In all hybrid profiles four CFRP mats with 100 mm of width and ~0.25 mm of thickness were used. Except for series S4, the introduction of the CFRP mats replaced the existing GFRP equivalents. Due to the manufacturer production procedure, series S4's CFRP reinforcement configuration was only possible by stitching it to the existing superficial GFRP mats. The configuration adopted in each series is presented in Figure 1 and described below:

- **Series S0**, a bare GFRP profile, was defined as the reference series;
- **Series S1** presented a set of two unidirectional CFRP mats in one flange and another set of two bidirectional CFRP mats in the other. Both sets of mats were introduced in the midline of the flanges aiming at maximizing saturation and mitigating delamination issues;
- **Series S2** presented a similar configuration of CFRP mats to that adopted in series S1, but in this case only unidirectional mats were used in both flanges;
- **Series S3** had similar fiber architecture to that of series S1 and S2, but two sets of bidirectional CFRP mats were used in both flanges. Due to saturation difficulties faced by the manufacturer with the coupled set of mats, one decided to separate the two CFRP mats: one at the outer face of the flange and the other in its midline;
- **Series S4** was designed with four CFRP bidirectional mats around the web-flange junction to increase the shear stiffness and strength of this particular (weaker) location.

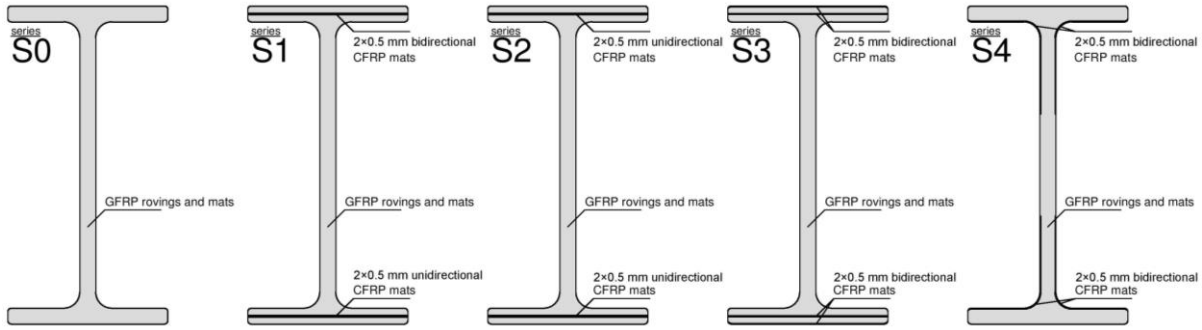

Figure 1: Reference GFRP and hybrid GFRP and CFRP pultruded experimental series.

For each series, specimens with the following lengths were cut from the reference and hybrid prototype profiles (three replicate specimens per length): (*i*) 60 cm – short columns, to study the local buckling modes; (*ii*) 200 cm – long columns, to study the global buckling modes; and (*iii*) 100 cm – intermediate columns, to assess the mixed global-local buckling modes.

Figure 2 illustrates the test setup and instrumentation used for each height tested. All columns were instrumented with displacement transducers next to the extremity sections and two out of three columns within each series were equipped with strain gauges at the mid height section. The test setup adopted presented slight differences for the different heights tested. Contrary to the intermediate and long columns, in which the end sections' rotation around the minor axis was set free, in the short columns this degree of freedom was restrained.

2.2 Summary of results

The typical experimental load *vs.* axial shortening and axial stress *vs.* strain curves exhibited by the short, intermediate and long columns of series S0 and S3 (as an example) are shown in Figure 3 to Figure 6. Corresponding numerical results, discussed later, are also shown.

Ultimate loads (P_{ult}) were defined as the maximum load carrying capacity exhibited in each test. The full-section elastic moduli (E_{fs}) were calculated using the linear part of the stress *vs.* strain data obtained from the strain gauge measurements. Finally, the critical buckling loads (P_{bk}) were computed using the Southwell plot method [7] (for the long and intermediate columns) and the modified Southwell plot method proposed by Barbero and Trovillion [8] (for the short columns). Since the long columns did not actually fail, their collapse load is not included in the summary of results (Table 1).

As shown in Table 1, the main advantage of introducing carbon fibers was the slight increase in the axial stiffness, in average 5% to 8% depending on the series (note that the replacement ratio of glass fibers by carbon fibers was low). On the other hand, the main drawback was the overall reduction of the load carrying capacity in terms of both critical and ultimate loads, more relevant for the lengths (short and intermediate columns) in which higher axial strain levels developed. In columns subjected to lower axial strains (long columns) the CFRP reinforcement was still effective for ultimate (buckling) limit states. This suggests that throughout the compressive test of the short and intermediate columns, as the average axial strain level increased, the interface between both materials was deteriorated, leading to the progressive delamination of the CFRP mats. This phenomenon seems to have had more impact in the hybrid series reinforced with bidirectional CFRP mats (series S3 and S4), which is consistent with the higher difficulty reported by the manufacturer in saturating the polymer matrix when using bidirectional mats.

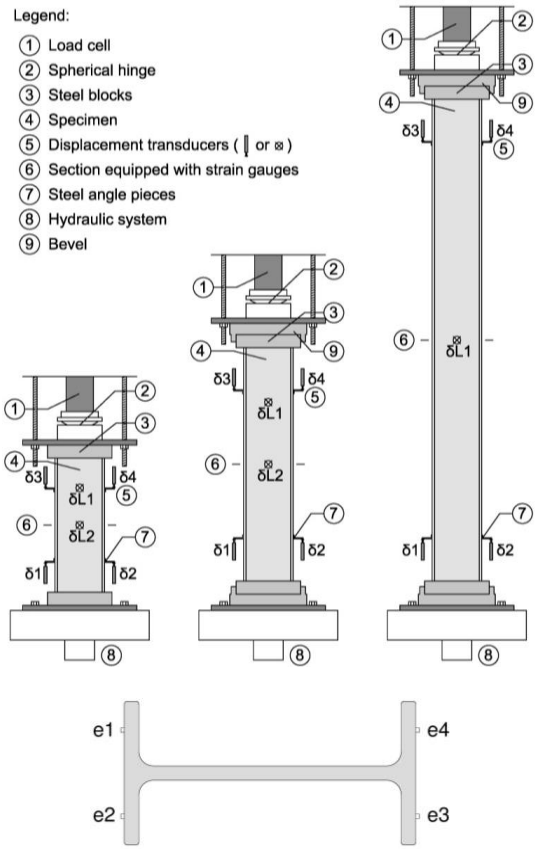

Figure 2: Test setup and instrumentation for each height tested; strain gauge position.

Table 1: Summary of average results of the experimental campaign.

Series	Length (m)	E_{fs} (GPa)	P_{bk} (kN)	P_{ult} (kN)
S0	60	37.4	690	734
	100	37.3	500	531
	200	35.3	134	-
S1	60	38.1	645	755
	100	39.5	545	511
	200	39.5	155	-
S2	60	38.5	624	668
	100	38.7	539	517
	200	38.2	152	-
S3	60	37.3	617	660
	100	41.4	487	458
	200	40.5	148	-
S4	60	39.6	683	634
	100	38.4	513	486
	200	41.2	155	-

The failure modes presented by each column were very consistent within each height, with all specimens generally exhibiting a single failure mode, despite the variations in ultimate and critical loads.

The governing failure mode of the **short columns** was caused by the local buckling of the flange, with symmetrical or anti-symmetrical mode shapes followed by partial or total web-flange separation (Figure 7a). This failure mode occurs due to high shear stresses developed in the web-flange junction after buckling is triggered [2].

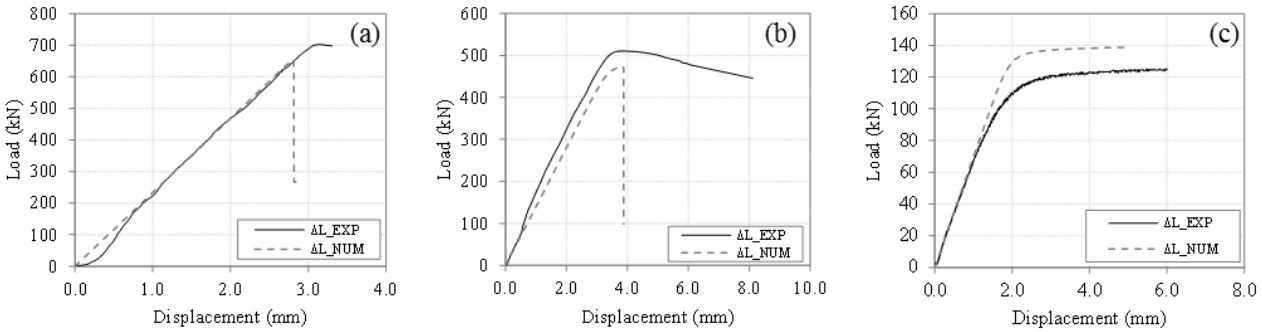

Figure 3: Load *vs.* axial displacement curves of (a) short, (b) intermediate, and (c) long columns - experimental (representative) and numerical (FE) curves (reference series S0).

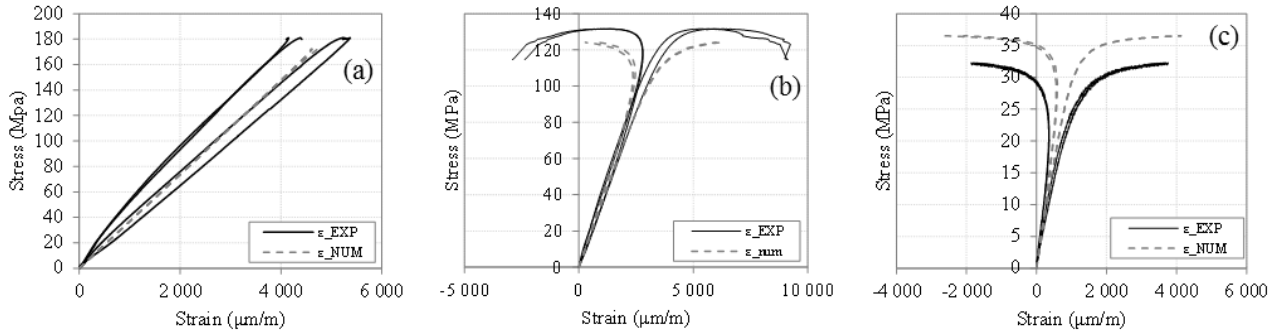

Figure 4: Average axial stress *vs.* strain measured in each strain gage curve of (a) short, (b) intermediate, and (c) long columns - experimental (representative) and numerical (FE) curves (reference series S0).

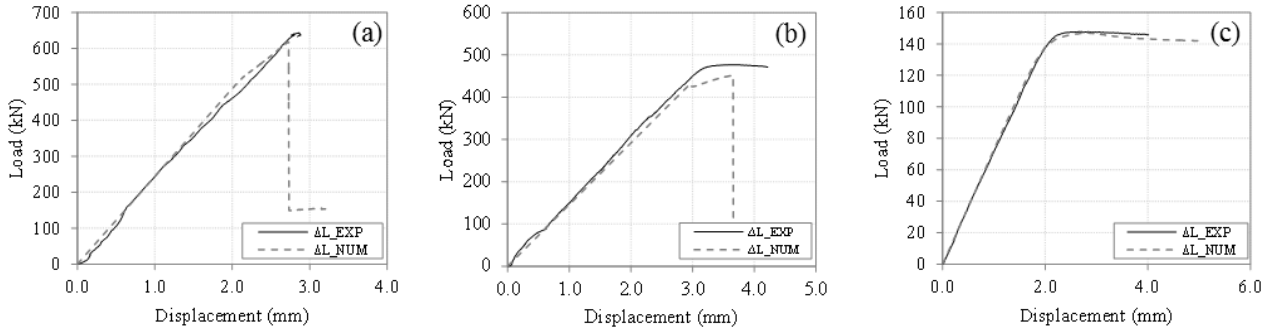

Figure 5: Load *vs.* displacement curves of (a) short, (b) intermediate, and (c) long columns - experimental (representative) and numerical (FE) curves (hybrid series S3).

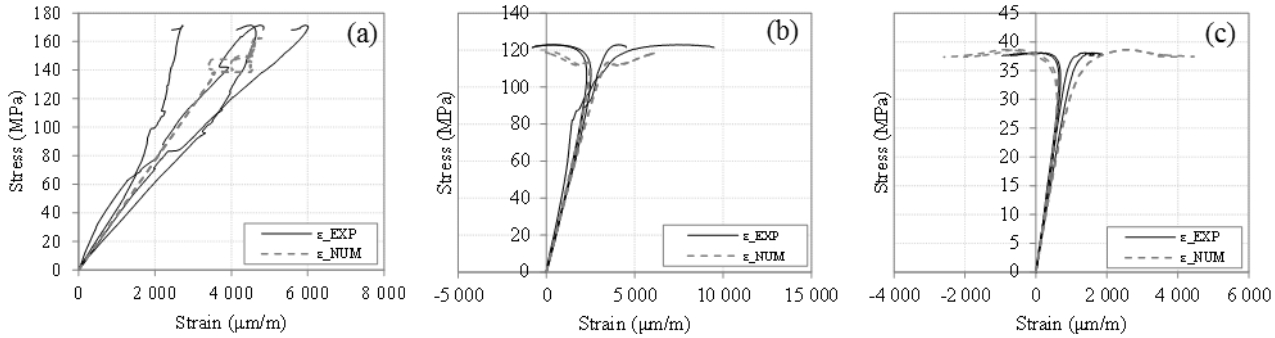

Figure 6: Average axial stress *vs.* strain measured in each strain gage curve of (a) short, (b) intermediate, and (c) long columns - experimental (representative) and numerical (FE) curves (hybrid series S3).

The failure mode of the **intermediate columns** comprised two different stages. In the first stage, columns buckled in a global mode shape, up to a lateral deflection of 5.0 to 10.0 mm; at the end of this stage the maximum load (P_{max}) was reached. In the second stage, the coupling between global and local modes and the progressive damage of the material were triggered and consequently specimens started losing their load carrying capacity (in an unstable buckling path). Finally, the collapse of the specimens occurred due to partial web-flange separation and/or flange crushing (Figure 7b).

The **long columns** did not collapse and thus it is more accurate to refer their buckling limit state instead of their failure mode. As expected, the long pultruded FRP columns presented global buckling around the minor axis (Figure 7c). The buckling path roughly

followed a hyperbola, asymptomatically tending to the critical load, which confirms the stable post-buckling path of the global buckling phenomenon in FRP pultruded columns. At the end of the test, columns were unloaded without any visible damage.

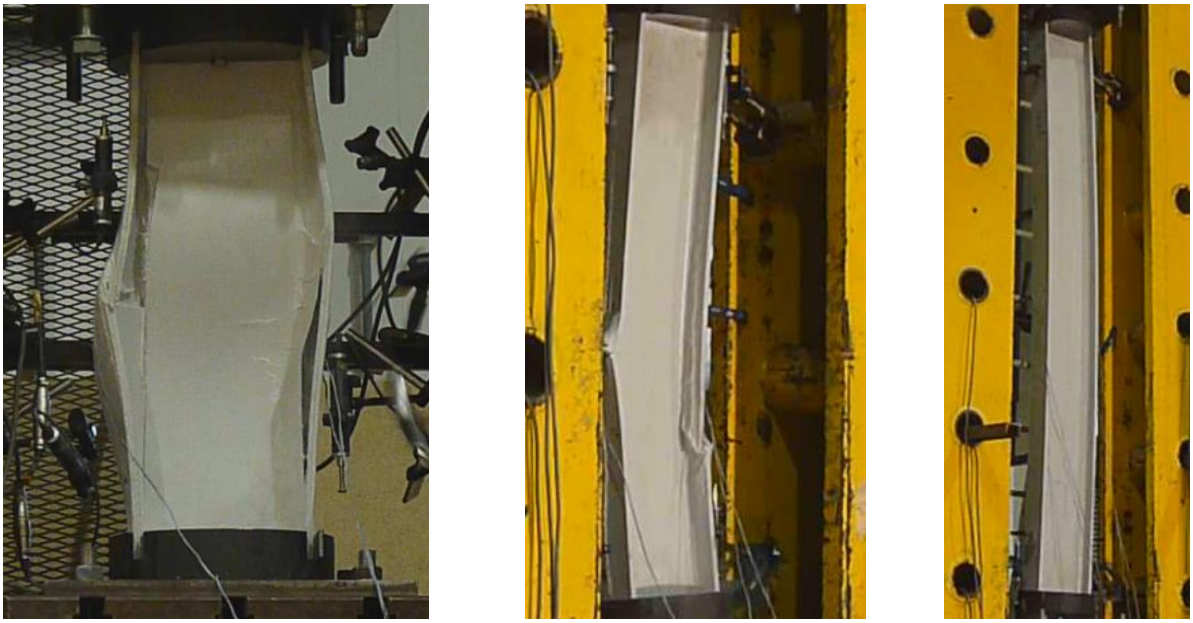

(a) (b) (c)

Figure 7: Failure modes exhibited by (a) short and (b) intermediate columns; ultimate limit state exhibited by (c) long columns.

3 MODEL DESCRIPTION

3.1 Mesh, load and boundary conditions

Finite element (FE) numerical models were developed using the commercial software ABAQUS [4]. Two different parts were modelled: (*i*) the I-section FRP pultruded profile, and (*ii*) the steel blocks. The steel blocks, with a diameter of 250 mm and a thickness of 27 mm, were meshed using eight-node solid elements with reduced integration (*C3D8R*) and were assigned a rigid body behavior. The I-section FRP profiles (200×100×10 mm) were meshed using eight-node continuum shell elements with reduced integration and three integration points across each layer's thickness (*SC8R*). The web and flanges' sections were modelled using a composite layup, which varied from series to series, according to the CFRP mats' configuration.

Apart from the web-flange junction, the FRP profiles were meshed uniformly with an element length-to-width ratio of approximately 10:5 (mm). In order to have only one element across the web thickness, the web-flange junction was meshed with an element length-to-width ratio of 10:10 (mm). Thus, the FRP pultruded profiles presented a total of 74 elements and 150 nodes in their cross-section.

Load and boundary conditions were applied directly to the steel blocks' rigid body reference point. Load was applied to the top steel block by means of a concentrated load in the linear buckling analyses and an imposed displacement in the nonlinear analyses. Restrained degrees of freedom were different for each column height according to the test setup illustrated earlier in Figure 2.

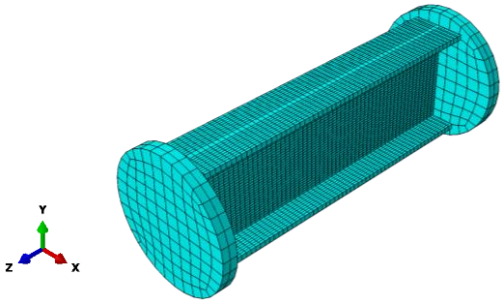

Figure 8: Example of FE mesh for short column specimen.

3.2 Material properties

The elastic properties of the three different types of composite layers constituting the profiles tested are presented in Table 2 and were defined based on the mechanical characterization tests performed. Strength properties are also listed in this table, where E_i is the Young's modulus in the i direction, ν_{ij} is the Poisson ratio between directions i and j, G_{ij} is the shear modulus in the ij plane, $S_{t,i}$ is the tensile strength in the i direction, $S_{c,i}$ is the compressive strength in the i direction, and S_{ij} is the shear strength in the ij plane. The three parts modelled (two steel blocks and one FRP profile) were connected using a surface-to-surface tie interaction.

Table 2: Elastic and strength properties of composite materials: input data for the FE models.

Material	E_1 (GPa)	E_2 (GPa)	ν_{12}	G_{12} (GPa)	G_{13} (GPa)	G_{23} (GPa)	$S_{t,1}$ (MPa)	$S_{c,1}$ (MPa)	$S_{t,2}$ (MPa)	$S_{c,2}$ (MPa)	S_{12} (MPa)
GFRP	36.6	10.8	0.266	3.65	3.65	1.60	365	468	85.8	110	20.1
Unidirectional CFRP	192.9	10.8[(1)]	0.266[(1)]	3.65 [(1)]	3.65 [(1)]	1.60[(1)]	1389	569[(3)]	85.8[(1)]	110[(1)]	20.1[(1)]
Bidirectional CFRP	95.9	95.9[(2)]	0.266	3.65	3.65	3.65	837	343	837	343	20.1[(1)]

[(1)] The referred test was not performed; the property was considered to be equal to that of the GFRP material.
[(2)] The referred test was not performed; the property was considered to be equal to that in the longitudinal direction.
[(3)] The referred test was not performed; compressive delamination strength was set as 41% of its corresponding tensile strength, according to [5].

3.3 Hashin material damage criterion

The Hashin damage initiation criterion, specifically developed for FRP composite materials, allows predicting the failure initiation of a given FRP member. It comprises four different initiation criteria: (*i*) fiber in tension; (*ii*) fiber in compression; (*iii*) matrix in tension and/or shear; and (*iv*) matrix in compression [4]. Once any of these initiation criteria is reached, the corresponding material stiffness is affected by a damage variable (d), which is automatically computed by ABAQUS according to the specified fracture energy (G). Figure 9 illustrates the standard evolution of a general damage variable. The fracture energy corresponds to the area under the equivalent stress *vs.* equivalent displacement curve in Figure 10. The interested reader should refer to [9], [10] for more information regarding the Hashin damage criterion development or to [11], [12] for more recent studies regarding its implementation in ABAQUS. According to the best of the authors' knowledge the estimation of the fracture energy of FRP composites is not yet standardized, namely for pultruded unidirectional laminates. Thus, in the present study the failure initiation strength was set as the maximum strength (indicated in Table 2) and the fracture energy was defined as the area under the stress *vs.* strain curves obtained from the mechanical characterization tests (Table 3).

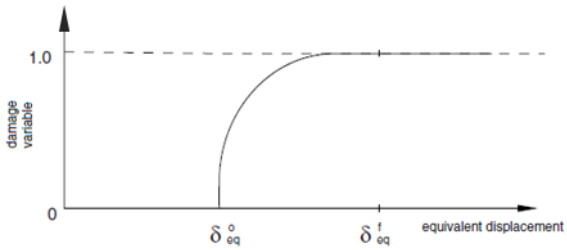

Figure 9: Damage variable as a function of equivalent displacement [4].

Figure 10: Equivalent stress *vs*. equivalent displacement [4].

Table 3: Fracture energy estimated for each material and failure mode.

Material	G_{ft} (N/mm)	G_{fc} (N/mm)	G_{mt} (N/mm)	G_{mc} (N/mm)
GFRP	2.38	5.28	0.424	0.948
Unidirectional CFRP	5.86	2.71	0.424	0.948
Bidirectional CFRP	4.28	1.98	4.28	1.98

Due to the convergence difficulties associated with softening analyses, the use of the damage stabilization option is recommended [4]. In this study, the value of 1.0×10^{-5} was used for all materials' viscosity coefficients. Since the continuum shell elements available in the ABAQUS element library do not allow for full integration, the use of enhanced hourglass control is recommended aiming at avoiding shear locking issues [4]. However, while for series S0 this option proved to be effective, for the hybrid series it led to severe convergence difficulties, and hence the authors decided not to use it in any series.

4 LINEAR BUCKLING ANALYSES

Since the global structural behavior presented by all hybrid series was roughly similar, in this paper only results obtained for series S0 (reference) and S3 (hybrid) are presented for comparison purposes. Series S3 was chosen over the remaining hybrid series since it was the one in which the CFRP mats' delamination was more easily identified in the experimental curves.

Eigenvalue linear buckling analyses were first performed aiming at determining each series' elastic buckling load *vs.* column height relation. They also enabled determining the buckled shapes of each buckling mode to be used as an initial imperfection in the nonlinear analyses performed afterwards. For each numerical model (series and height), the first buckling mode and its corresponding critical load were determined. Table 4 lists the results obtained for each height tested (series S0 and S3), where $P_{bk,h}$ (h = 60, 100, 200 cm) is the linear elastic critical buckling load of the first buckling mode. Figure 11 illustrates the first buckling modes' deformed shapes for each column height tested. Since they do not differ significantly from series to series, only the plots for series S0 are presented.

It can be seen that short columns presented a local buckling deformed shape with two half-waves along the profile length and one across the web height (Figure 11a). Intermediate columns presented a mostly global buckling mode with a slight bending of the web in the transverse direction (mixed local-global buckling mode) more relevant in the sections next to the mid-height (Figure 11b). Long columns presented a pure global buckling mode with negligible section deformation when comparing to the overall column deformation (Figure 11c).

The results obtained show that as long as delamination does not occur, the CFRP reinforcement has a positive effect in the structural member, regardless of the column height.

It is also shown that even though bidirectional mats are used in the flanges, they have very little influence in the local buckling critical load of short columns; they are more effective in increasing the critical load of members subjected to global buckling phenomena.

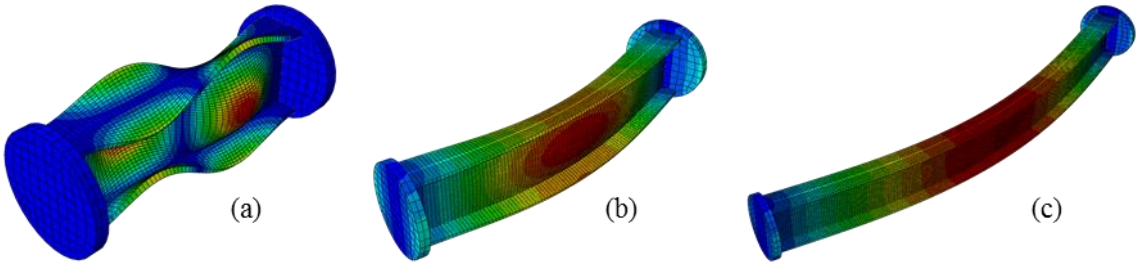

Figure 11: Deformed shape of the lowest buckling modes for (a) short, (b) intermediate, and (c) long columns.

5 PROGRESSIVE FAILURE ANALYSES

After completing the linear buckling analyses, nonlinear analyses were performed using the Hashin material damage criterion. In this section the numerical results are first compared with the experimental data described in section 2 in order to validate the numerical models, namely in what concerns the variation of load against axial displacement, the stress *vs.* strain behavior and the buckling behavior. Next, additional information is extracted from the calibrated models, namely regarding the progressive failure behavior.

Figure 3 to Figure 6 plot the numerical results obtained (together with the experimental data) in terms of load *vs.* axial displacement and axial stress *vs.* average strain for the columns from the reference series (S0) and the hybrid series (S3). The comparison between numerical and experimental ultimate loads is presented in Table 5. For the short and intermediate columns (60 and 100 cm) the ultimate load corresponds to the collapse load, while for the long columns (200 cm) this comparison is performed in terms of buckling load.

It can be seen that the numerical curves plotted in Figure 3 to Figure 6, as well as the ultimate loads presented in Table 5, present a reasonably satisfactory agreement with their experimental counterparts, with relative differences ranging from 1.5% to 11.1%. The results obtained highlighted the high sensitivity of the axial strains measured in the columns to the test setup, which was more restraining for the short columns than for the intermediate and long columns. Consequently, the axial strains measured in the short columns presented a higher scatter (that is naturally not replicated in the numerical curves); in opposition, for the intermediate and long columns the evolution of axial strains was much smoother.

Figure 6a and Figure 6b indicate that both the delamination strength and its corresponding fracture energy may not have been fully accurately estimated. In fact, the experimental results suggest that the CFRP mat's delamination occurs earlier (for an average full section axial stress of 80 MPa) than predicted by the numerical models and that the phenomenon seems to be more progressive than that simulated by the numerical models. Thus, future calibrations should assess the effect of reducing the compressive fiber initiation criterion and increasing its corresponding fracture energy; this should provide a smoother delamination simulation along the loading path. Also, in what regards short and intermediate columns, the overall displacement at failure was slightly higher in the tests. This indicates that either the shear strength (which governs these failure modes) or the matrix tension fracture energy should be slightly higher than considered.

Table 4: Linear buckling analysis results.

Series	$P_{bk,60}$ (kN)	$P_{bk,100}$ (kN)	$P_{bk,200}$ (kN)
S0	661	485	141
S3	685	522	152
Diff.	3.6%	7.6%	7.8%

Table 5: Comparison between experimental and numerical loads.

Series	Length (cm)	$P_{ult,exp}$ (kN)	$P_{ult,num}$ (kN)	Diff.
S0	60	734	654	10.9%
	100	531	472	11.1%
	200	134	141	5.2%
S3	60	660	618	6.4%
	100	458	451	1.5%
	200	148	152	2.7%

Figure 12 and Figure 13 illustrate the envelope of the damaged zones (respectively in the brink of collapse and after failure) of the governing Hashin criterion (matrix tension and shear) for both short and intermediate columns of series S0 (in these figures the red color indicates a fully damaged element, d = 1.0, while the blue color indicates the undamaged areas, d = 0.0). The long columns of the reference profile did not exhibit any damage zones for the maximum imposed axial displacement (5 mm), which is also in agreement with the test results.

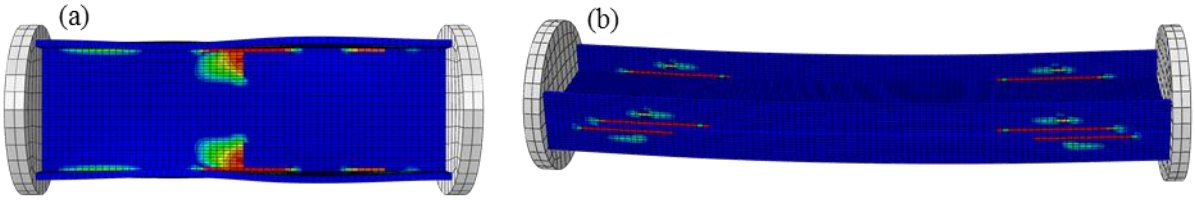

Figure 12: Damaged areas in the brink of collapse for (a) short, and (b) intermediate columns (reference series S0).

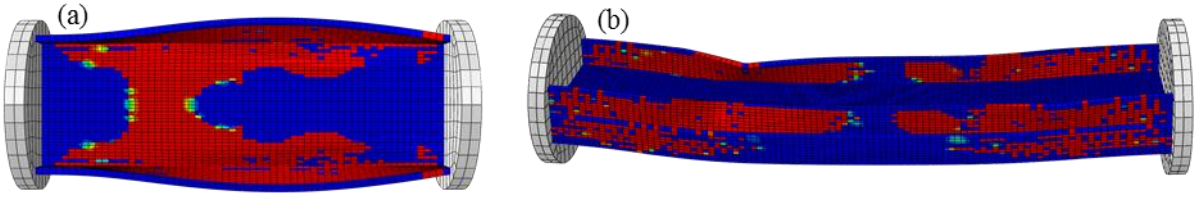

Figure 13: Damaged areas after failure for (a) short, and (b) intermediate columns (reference series S0).

As shown in Figure 12, for both short and intermediate lengths, the damaged areas concentrate in the web-flange junctions. Nevertheless, for short columns the web elements are governing, while for intermediate columns the flange elements are more prominent to failure. Figure 13 shows that, after failure, the damaged zones of the short columns comprise a large area in both the flanges and the web, while in the intermediate columns the damaged zones are mainly restricted to the flanges.

Regarding the delamination behavior, Figure 14 to Figure 16 show the triggering and the state of the fiber compression criterion at the brink of failure (with the same color scale as in Figure 12 and Figure 13). This parameter illustrates the delamination evolution of the CFRP mats with the applied load for short, intermediate and long columns of series S3. As expected, short columns seem to be the most affected by the delamination phenomenon, both due to the higher axial strains they are subjected to and to the fact that the local buckling

phenomenon does not introduce a significant eccentricity in the deformed shape. On the other hand, intermediate and long columns are affected only in the most compressed part of each flange due to the bending stress component arising from the column imperfection shape. Since the FE model of the long columns did not show any signs of collapse, only the triggering of the delamination is plotted in Figure 16. With the increase of axial displacement imposed, the lateral deflection also increases and the delaminated areas further develop.

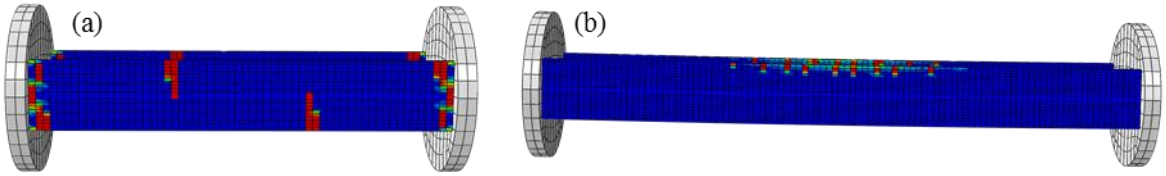

Figure 14: Delamination triggering for (a) short – 0.83 P_{ult} – and (b) intermediate – 0.93 P_{ult} – columns (hybrid series S3).

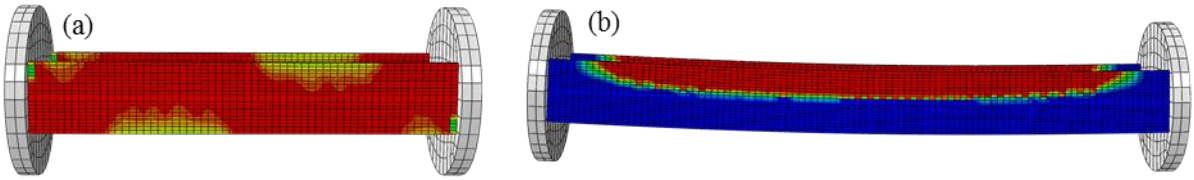

Figure 15: Delamination state in the brink of failure for (a) short, and (b) intermediate columns (hybrid series S3).

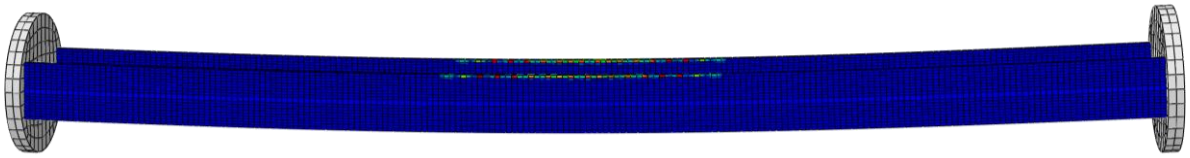

Figure 16: Delamination triggering for long columns.

6 CONCLUSIONS

This paper presented results of experimental and numerical investigations about the structural behavior of hybrid FRP pultruded columns. Particular attention was given to the progressive failure, which was numerically analyzed using the Hashin material damage criterion. The following main conclusions can be drawn:

- Experimental results obtained showed that the introduction of CFRP fibers in bare GFRP profiles effectively increases the overall compressive stiffness of columns for serviceability load levels.
- The ultimate behavior of the reference and hybrid profiles showed that the introduction of CFRP fibers might decrease the load carrying capacity of compressive members (both in terms of buckling and collapse loads), namely in short and intermediate columns.
- Delamination between the GFRP and CFRP interfaces has likely occurred throughout the tests of short and intermediate columns. This is supported by both the decrease of the load carrying capacity of hybrid columns and the stress *vs.* strain curves of series S3, which presented considerable perturbations around an average axial stress of 80 MPa.
- Numerical FE models using progressive failure analyses presented a reasonably good agreement with the experimental data, with relative differences only up to 11.1% in what concerns the ultimate loads.

- The Hashin material damage criterion has shown to adequately simulate both the material failure and the delamination; the failure modes obtained in the numerical models were also consistent with those observed experimentally.
- Regarding the properties adopted, some calibration using curve fitting procedures might be required aiming at performing accurate parametric studies, namely with respect to the CFRP compressive (delamination) strength and its corresponding fracture energy. Also the GFRP shear strength and its matrix tension fracture energy might need to be slightly increased in future simulations.
- Despite that the local buckling phenomenon does not allow for significant stress redistribution (and thus the Tsai-Hill index might give an accurate estimate of the ultimate load), the achievements made in this numerical study may provide a useful tool and a strong basis for modelling different FRP structures and load configurations involving higher stress redistribution (for instance, the web-crippling phenomenon).

REFERENCES

[1] J. Correia, "GFRP pultruded profiles in civil engineering: hybrid solutions, bonded connections and fire behaviour," PhD Thesis, Instituto Superior Técnico, Lisbon, 2008.

[2] M. M. Correia, F. Nunes, J. R. Correia, and N. Silvestre, "Buckling Behavior and Failure of Hybrid Fiber-Reinforced Polymer Pultruded Short Columns," *J. Compos. Constr.*, Vol. 17, no. 4, pp. 463–475, 2013.

[3] L. A. Fernandes, F. Nunes, N. Silvestre, J. R. Correia, and J. Gonilha, "Web-crippling of GFRP pultruded profiles. Part 2: Numerical analysis and design," *Compos. Struct.*, Vol. 120, pp. 578–590, 2015.

[4] Simulia, "Abaqus 6.11." Simulia, 2011.

[5] F. F. Nunes, "Structural behavior of GFRP pultruded profiles reinforced with CFRP mats: experimental characterization and numerical modelling" (in portuguese), Instituto Superior Técnico, 2012.

[6] W. F. Ragheb, "Hybridization Effectiveness in Improving Local Buckling Capacity of Pultruded I-Beams," *Mech. Adv. Mater. Struct.*, Vol. 17, no. 6, pp. 448–457, 2010.

[7] R. V. Southwell, "On the Analysis of Experimental Observations in Problems of Elastic Stability," *Proc. R. Soc. A Math. Phys. Eng. Sci.*, Vol. 135, no. 828, pp. 601–616, 1932.

[8] E. J. Barbero and J. Trovillion, "Prediction and measurement of the post-critical behavior of fiber-reinforced composite columns," *Compos. Sci. Technol.*, Vol. 58, no. 8, pp. 1335–1341, 1998.

[9] Z. Hashin and A. Rotem, "A Fatigue Failure Criterion for Fiber Reinforced Materials," *J. Compos. Mater.* , Vol. 7 , no. 4 , pp. 448–464, 1973.

[10] Z. Hashin, "Failure Criteria for Unidirectional Fiber Composites," *J. Appl. Mech.*, Vol. 47, no. 2, pp. 329–334, 1980.

[11] E. J. Barbero, F. A. Cosso, R. Roman, and T. L. Weadon, "Determination of material parameters for Abaqus progressive damage analysis of E-glass epoxy laminates," *Compos. Part B Eng.*, Vol. 46, pp. 211–220, 2013.

[12] A. M. Girão Coelho, J. Toby Mottram, and K. A. Harries, "Finite element guidelines for simulation of fibre-tension dominated failures in composite materials validated by case studies," *Compos. Struct.*, Vol. 126, pp. 299–313, 2015.